

# Relativistic Attosecond Electron Pulses from a Photocathode Radio-Frequency Gun

Cheng Li<sup>ID</sup>, Wenxing Wang<sup>ID</sup>, Haoran Zhang<sup>ID</sup>, Zixin Guo, Shimin Jiang<sup>ID</sup>, Zhigang He<sup>ID</sup>,<sup>\*</sup>  
Shancai Zhang<sup>ID</sup>, Qika Jia, Lin Wang, and Duohui He

National Synchrotron Radiation Laboratory, University of Science and Technology of China, Hefei, Anhui,  
230029, China



(Received 1 July 2021; revised 24 September 2021; accepted 15 October 2021; published 2 November 2021)

The interaction of light and electrons has been one of the important frontiers for generating ultra-short electron pulses in free-electron lasers, ultrafast science, and dynamical analysis of matter. However, the generation of a relativistic attosecond electron beam remains a challenge. In a photocathode radio-frequency (rf) gun, this work identifies a regime for obtaining an isolated or a train of relativistic attosecond electron pulses. A photoelectron beam is generated from the cathode under the illumination of a driving laser pulse in the electron gun, which is subsequently microbunched to optical wavelength scale by the field of a synchronized radially polarized laser (RPL) pulse that is focused near the cathode surface. The rf field in the gun cavity simultaneously accelerates the electron pulse to several MeV. The rf field causes a velocity differential inside the electron beam as it passes into the region near the focal point of the RPL (microbunching is processed), and the microbunch at the head is substantially faster than that at the tail. Using this knowledge, the spacing between consecutive microbunches, referred to as bunch spacing, may be controlled across a wide range by regulating the velocity difference, which can be accomplished by tuning the phase and amplitude of the rf field. Numerical simulations show that a train of attosecond bunches with tunable bunch spacing can be generated using realistic laser parameters corresponding to current GW-power-level laser systems, and an isolated attosecond pulse can be obtained when the driving laser pulse is about 50 fs. This regime may result in opportunities in ultrafast electron diffraction and microscopy, free-electron lasers, and other applications that require high-energy electrons with the temporal structure of single-cycle light.

DOI: 10.1103/PhysRevApplied.16.054007

## I. INTRODUCTION

X-ray and electron beams are important probes for understanding the microscale world and ultrafast processes. Compared with an X-ray beam, a relativistic electron beam with subpicometer de Broglie wavelength can achieve higher spatial resolution detection. By using pump-probe technology, MeV ultrafast electron diffraction (UED) has revealed several ultrafast dynamic processes that have not been seen before [1–4], providing a tool for the development of research frontiers. In order to further extend and improve its function, shorter electron bunches are in great demand for achieving a higher time resolution. In x-ray free-electron laser (FEL) facilities, radiation is generated by sending a relativistic electron beam through a series of undulators [5–7], so the x-ray pulse width is largely dependent on the pulse width of the electron beam.

In recent years, attosecond science has brought many opportunities for time-resolved spectroscopy and imaging technology [8,9], and also promoted the development of

attosecond electron pulses [10–17]. Optical field modulation is widely studied in obtaining attosecond electron bunches [11–14] because of the ultrashort period length of optical pulses. The physics behind this effect is simple. Electrons at different positions in the optical wavelength are accelerated or decelerated under the action of the optical field, and velocity difference is introduced in the beam. After a certain drift distance, the velocity modulation transforms into density modulation, which means that the electron beam is microbunched at the optical frequency leading to the generation of a train of attosecond electron pulses. The key to this physical process is how to prevent the periodic electromagnetic acceleration and deceleration of the propagating electrons in the optical field cycles from canceling out after passing through the laser focus. To achieve this goal, researchers have contributed various ideas. A thin membrane is introduced into the transport line of the electron beam. The membrane is also transparent to the laser beam, but a refractive index of approximately 2 in combination with thin-layer interferences generates a phase shift between the incoming and outgoing electromagnetic waves. Therefore, the periodic electromagnetic acceleration and deceleration of the

\*hezhg@ustc.edu.cn

propagating electrons in the optical field cycles before and after the membrane do not cancel out after passage through the laser focus [11]. Two optical fields at different frequencies are used to form a ponderomotive force in the direction of electron propagation and make the propagation velocity of the traveling wave synchronized to the electron velocity, leading to the generation of an optical standing wave in the electrons' rest frame [12]. In order to obtain an isolated attosecond electron pulse rather than a pulse train, the two methods mentioned above have been extended. For the former, a single-cycle modulation laser pulse is adopted [13]. An additional third laser pulse with different frequency is introduced in the latter to form a transverse momentum modulation in the electron beam, which leads to microbunches in the pulse train being separated in the transverse space [14]. These demonstrations are all carried out for nonrelativistic electron beams. However, these above methods put an extremely high demand on the optical pulse power in order to bunch the relativistic electron beam.

At present, MeV ultrafast electron diffraction facilities, in which the electron beam is generated in a photocathode radio-frequency (rf) gun, can provide electron bunches of approximately 20 fs with the help of the magnetic compression technique [18,19]. Furthermore, the experimental demonstration of a Coulomb-driven bunch compression process opens a way to obtain shorter bunches in UED facilities [20]. However, it is still an open challenge to generate subfemtosecond electron pulses in a photocathode rf gun.

## II. PRINCIPLE

In this paper, we identify a regime to generate an isolated or a train of relativistic attosecond electron pulses in a photocathode rf gun. The cathode is a smooth oxygen-free copper surface, which can be considered as an ideal mirror for an infrared laser. A schematic illustration of the proposed setup is shown in Fig. 1(a). A horizontally polarized laser at a central wavelength of 800 nm is split into two pulses. One passes third-harmonic generation (THG) to generate a 266.7-nm ultraviolet (UV) pulse, which is used to drive the photocathode for photoelectron bunch emission. The other is converted into a radially polarized laser (RPL) pulse by a commercial vortex wave plate (the transmission efficiency can reach 99%). The RPL is then focused by an off-axis parabolic (OAP) to form an axial optical field in the region of the focal point, and this axial field can interact with the electron beam [21–24]. The synchronization of these two laser pulses can be controlled by the optical delay line. In order to get a high interaction efficiency, the RPL is focused after being reflected by the cathode surface, so that it moves in the same direction as the electron beam. The cathode surface is very close to the focal point. As a boundary, it breaks the symmetry of

the periodically axial electric field. Therefore, the electrons can be accelerated or decelerated (energy modulation) and then bunched into ultrashort microbunches (density modulation). The rf field in the gun cavity simultaneously accelerates the electron pulse to several MeV. When the beam moves into the region near the focal point of the RPL, there is a velocity difference inside it caused by the rf field, and the microbunch at the head is substantially faster than that at the tail. Thus, the spacing between consecutive microbunches, referred to as bunch spacing, may be controlled across a wide range by regulating the velocity difference, which can be accomplished by tuning the phase and amplitude of the rf field. Furthermore, the bunch spacing can be optimized to about 10 times the RPL wavelength, and an isolated attosecond electron bunch can be generated when the bunch length at the beginning of the bunching process is shorter than 2 times the bunch spacing.

## III. NUMERICAL CALCULATION

Due to the phase slippage effect caused by the inconsistency between the speed of electrons and light, it is difficult to get straightforward analytical estimates for the entire physical process. Therefore, in the following, we use numerical calculation results to illustrate this process. The fields of a RPL with wavelength  $\lambda$  and wave number  $k = 2\pi/\lambda$  can be written as [25]

$$E_r^r = \frac{r}{w_0} E_0 \frac{w_0^2}{w^2} e^{-\frac{r^2}{w^2}} \operatorname{sech} \frac{\omega t - kz}{\xi_0} \cos \psi, \quad (1)$$

$$E_z^r = \frac{w_0}{Z_R} E_0 \frac{w_0^2}{w^2} e^{-\frac{r^2}{w^2}} \operatorname{sech} \frac{\omega t - kz}{\xi_0} \times \left[ \left( 1 - \frac{r^2}{w^2} \right) \sin \psi - \frac{z}{Z_R} \frac{r^2}{w^2} \cos \psi \right], \quad (2)$$

$$B_\theta^r = E_r^r / c, \quad (3)$$

where  $\operatorname{sech}(\omega t - kz/\xi_0)$  is the pulse envelope,  $E_0$  is the field amplitude,  $\psi = \omega t - kz + 2\phi_G - [(z - L)/Z_R](r^2/w^2) + \phi_0$  is the field phase,  $\phi_G = \operatorname{atan}[(z - L)/Z_R]$  is the Gouy phase shift,  $Z_R = (\pi w_0^2/\lambda)$  is the Rayleigh length,  $w = w_0 \sqrt{1 + [(z - L)^2/Z_R^2]}$  and  $w_0$  are the beam radius and the beam radius at the waist, respectively,  $L$  is the focus position as shown in Fig. 1(a), and  $\omega$  is the angular frequency.  $\xi_0 = \{\omega\tau/\operatorname{acosh}[\exp(1)]\}$  is a parameter related to the pulse duration  $\tau$ , and  $c$  is the light velocity in vacuum. The power of the RPL is

$$P = \frac{\pi w_0^2 m_0^2 c^4 k^2}{8\eta_0 e^2} a_0^2, \quad (4)$$

where  $\eta_0 = 120\pi\Omega$  is the vacuum impedance,  $a_0 = [(eE_0)/(m_0 c^2 k)]$  is the normalized vector potential, and  $e$  and  $m_0$  are the charge and rest mass of an electron, respectively.

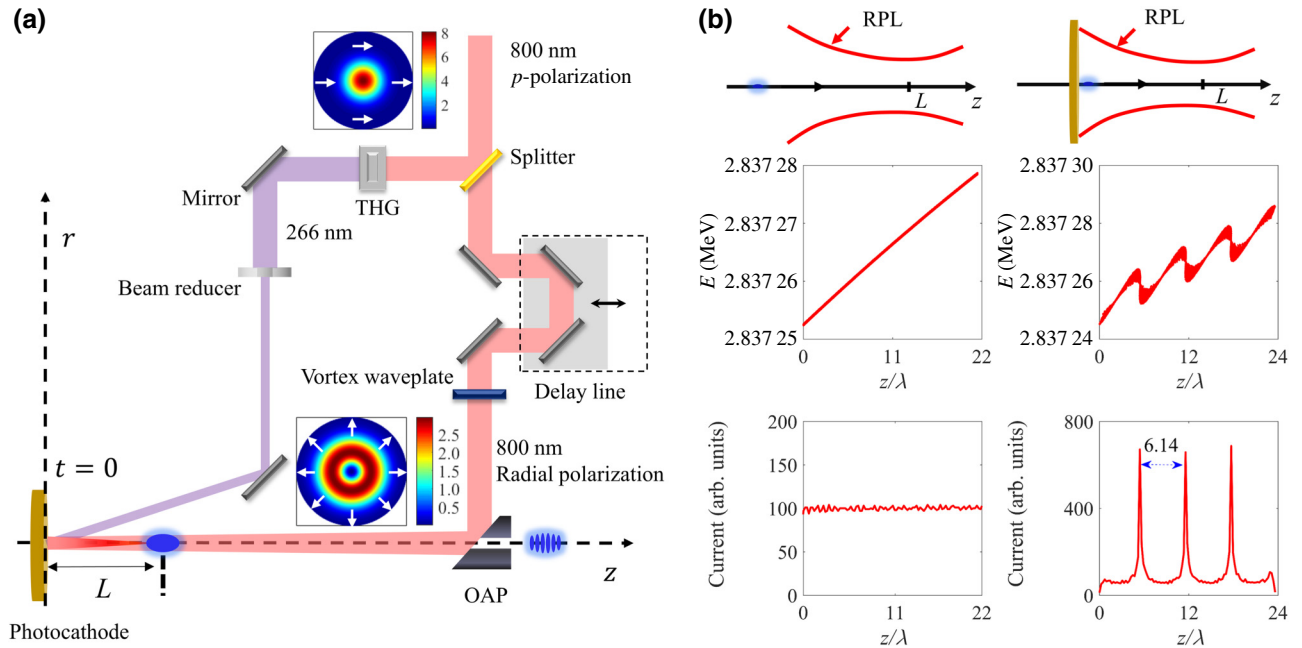


FIG. 1. (a) The schematic layout and (b) the phase space and current distribution of an electron beam after interaction with a RPL, for two cases: with (right column) and without (left column) a cathode boundary.

As for rf fields, most rf guns use the  $\text{TM}_{011}$  mode whose nonzero field components are [26]

$$E_z^{\text{rf}} = E_{01} J_0(k_{01}r) \cos(k_z z) \cos(\omega_1 t + \phi_{01}), \quad (5)$$

$$E_r^{\text{rf}} = k_z E_{01} J_1(k_{01}r) \sin(k_z z) \cos(\omega_1 t + \phi_{01}), \quad (6)$$

$$B_\theta^{\text{rf}} = k_z / c E_{01} J_1(k_{01}r) \cos(k_z z) \sin(\omega_1 t + \phi_{01}), \quad (7)$$

where  $E_{01}$  is the field amplitude,  $k_{01}$  is the 1st zero of the 0th-order Bessel function,  $\omega_1$  is the rf angular frequency,  $k_z = \pi/l$  is the longitudinal wave number, and  $l$  is the cavity length.

In the calculation, a 1.6-cell, S-band (2856-MHz) gun is used. The parameters of the RPL are set as  $\lambda = 0.8 \mu\text{m}$ ,  $\phi_0 = 0$ ,  $\tau = 1 \text{ ps}$ ,  $w_0 = 10 \mu\text{m}$ , and  $L = 70 \mu\text{m}$  in the full text. For a larger focus position  $L$ , the average energy of the electron beam is higher at this position, and a more intense RPL should be used to bunch the electron beam while the laser-induced damage threshold of the copper surface must be taken into account. In vacuum condition, the multipulse laser-induced damage threshold of the copper surface could be twice as high as that in air, and the measured value is about  $1.44(+1.44, -0.76) \text{ J/cm}^2$  for an infrared laser when the pressure is  $5 \times 10^{-5} \text{ Pa}$  [27]. For the photocathode rf gun, the background pressure is about  $1 \times 10^{-8} \text{ Pa}$ , so we set a maximum limit of  $a_0 = 0.0018$ , which corresponds to laser energy density  $F \sim 1.47 \text{ J/cm}^2$  and  $F \propto a_0^2$ .

Firstly, we discuss the interaction of the RPL and electron bunch in the rf gun, and two scenarios with and

without a cathode boundary are considered, as shown in Fig. 1(b). The parameters of the rf field are  $E_{01} = 60 \text{ MV/m}$ ,  $\phi_{01} = 280^\circ$ . If an electron bunch interacts with a RPL over an infinite region ( $z = -\infty$  to  $\infty$ ), it will experience both accelerating and decelerating phase regions of the laser fields, and then the net energy gain is zero [see the middle panel of the left-hand column of Fig. 1(b)], which means that the electron bunch cannot be modulated [see the bottom panel of the left-hand column of Fig. 1(b)]. When the photocathode is introduced as a boundary, the interaction distance is limited to a finite region around the laser focus. In this way, the electron bunch energy can be modulated [see the middle panel of the right-hand column of Fig. 1(b)], and the density modulation can be formed after a certain drift distance [see the bottom panel of the right-hand column of Fig. 1(b)].

Figure 2 shows the bunching results of an electron beam for different rf field amplitudes and phases. As shown in Fig. 2(a),(d),(g), the optical field introduces an energy modulation into the electron beam, which gradually transforms into density modulation. Meanwhile, the rf field makes the electrons at the head move faster than those at the tail, resulting in the stretching of the electron beam, which makes the bunch spacing longer and longer until the beam is accelerated to relativistic speed and the density distribution is frozen. The elongation of bunch spacing is determined by the velocity difference within the electron beam during the bunching process. As shown in Fig. 2(a)–(f), the bunch spacing varies with the

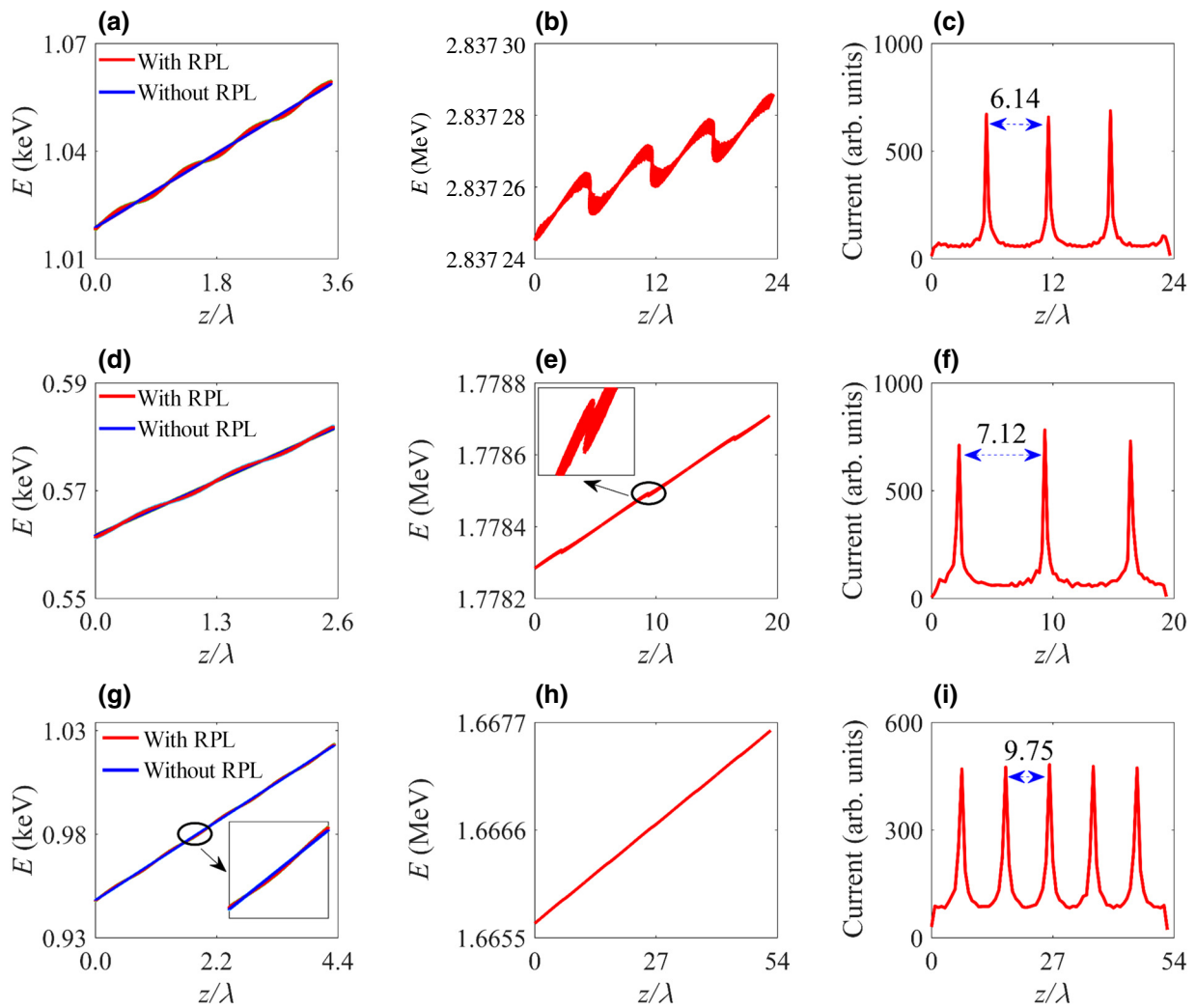


FIG. 2. Longitudinal phase space of the electron beam at the beginning of electron-laser interaction (a),(d),(g) and after the interaction and rf acceleration (b),(e),(h). Current distribution of the bunched electron beams (c),(f),(i). (a)–(c)  $a_0 = 0.0018$ ,  $E_{01} = 60 \text{ MV/m}$ ,  $\phi_{01} = 280^\circ$ ; (d)–(f)  $a_0 = 0.0015$ ,  $E_{01} = 40 \text{ MV/m}$ ,  $\phi_{01} = 280^\circ$ ; (g)–(i)  $a_0 = 0.0018$ ,  $E_{01} = 40 \text{ MV/m}$ ,  $\phi_{01} = 300^\circ$ . The beam head is on the right-hand side and the beam tail is on the left-hand side, also for the subsequent figures.

rf field amplitude. For higher field amplitude, the average energy of the electron beam is higher at the beginning of electron-laser interaction. Thus, the velocity difference is smaller, and the bunch spacing is shorter. Based on the same principle as above, it is not difficult to see that the bunch spacing of the electron beam can also be tuned by adjusting the phase of the rf field, as seen in Fig. 2(d)–(i).

Hence, the bunch spacing can be optimized to several times the RPL wavelength, and an isolated attosecond electron bunch can be generated when the driving laser pulse length is set as an appropriate value, as shown in Fig. 3. The parameters are set as follows:  $a_0 = 0.0018$ ,  $E_{01} = 60 \text{ MV/m}$ ,  $\phi_{01} = 280^\circ$ . The driving laser pulse is 50 fs, which can be achieved by a commercial laser system. When the rf parameters are set as in Fig. 2(g)–(i), the driving laser pulse width for obtaining an isolated electron pulse can be increased to about 70 fs.

#### IV. SIMULATION WITH SPACE CHARGE EFFECT

So far, the calculation results have not considered the space charge effect. In the following, we demonstrate the proposed scheme by using a three-dimensional relativistic

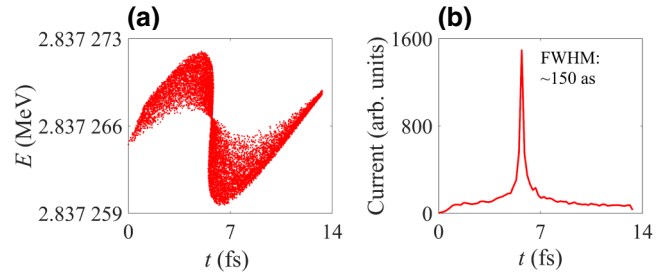


FIG. 3. The phase space (a) and current distribution (b) of the electron beam.

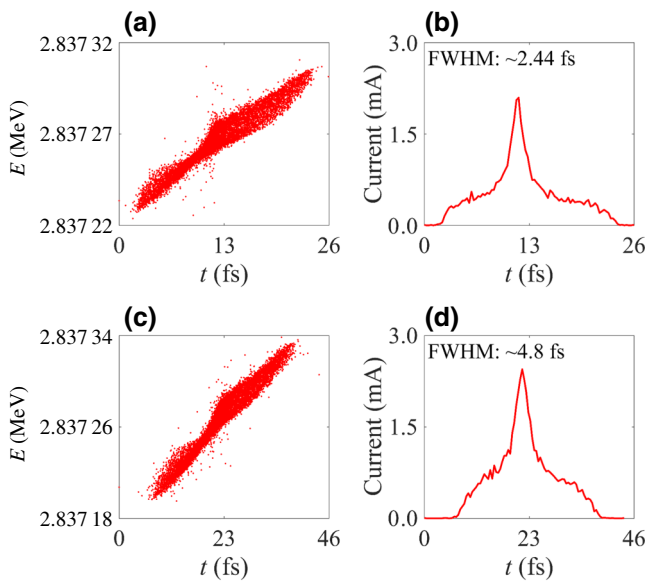


FIG. 4. Longitudinal phase space (a),(c) and current distribution (b),(d) of the electron beam. (a),(b) Charge: 0.0125 fC; (c),(d) charge: 0.025 fC.

particle tracing simulation with the General Particle Tracer code [28]. The space charge effect is included and the simulation is performed for the above scenario of generating an isolated attosecond pulse. The initial electron bunch follows uniform distributions in both longitudinal and radial directions within the bunch. The radius and length are set to  $5 \mu\text{m}$  and 50 fs, respectively, and the initial kinetic energy  $h\nu - \Phi_{\text{eff}} = 0.4 \text{ eV}$ , where  $h\nu$  is the UV laser photon energy and  $\Phi_{\text{eff}}$  is the effective work function of copper. Using the thermal emittance calculation model [29] given by  $\varepsilon_n = \sigma_x \sqrt{[(h\nu - \Phi_{\text{eff}})/(3m_0 c^2)]}$ , where  $m_0 c^2$  is the electron rest mass energy and  $\sigma_x$  is the transverse rms laser beam size on the cathode, we get that the initial thermal emittance is  $1.275 \times 10^{-3} \text{ mm mrad}$ .

As seen in Fig. 4, the electron bunch is broadened due to the space charge effect. In order to get subfemtosecond electron beams, the bunch charge must be very low. It is worth noting that, for other methods of generating

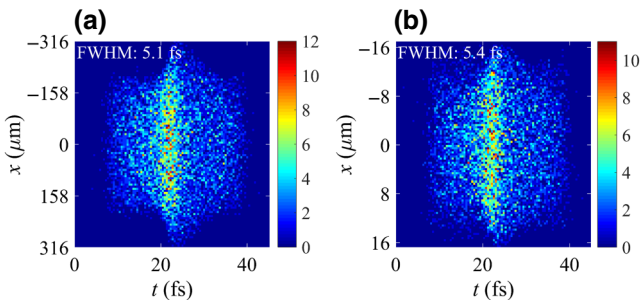


FIG. 5. The electron beam distribution at 0.55 m away from the cathode surface without  $B_z$  (a) and with  $B_z = 0.162 \text{ T}$  (b).

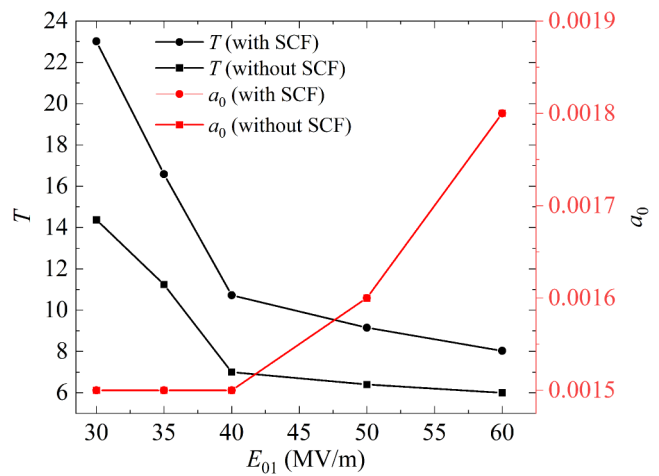


FIG. 6. The ratio of bunch spacing to RPL wavelength as a function of rf field amplitude with optimized laser power ( $\phi_{01} = 280^\circ$ ).

attosecond electron bunches, the generated electron packets consist of very few or even single electrons [10–17].

The transverse size of the electron bunch is expanded by the action of the transverse field, as seen in Fig. 5(a), where the bunch charge is 0.025 fC. So a solenoid field is added into the simulation, which is a conventional configuration of a photocathode rf gun. The center of this field is set at 0.2 m away from the cathode surface, and the effective length is 0.2 m. As shown in Fig. 5(b), with this external magnetic field, the electron beam is focused to a smaller size at a specific position, and an isolated electron bunch with a full width at half maximum (FWHM) of 5.4 fs is obtained.

Figures 6 and 7 show the ratio  $T$  of bunch spacing to RPL wavelength as a function of rf field amplitude and

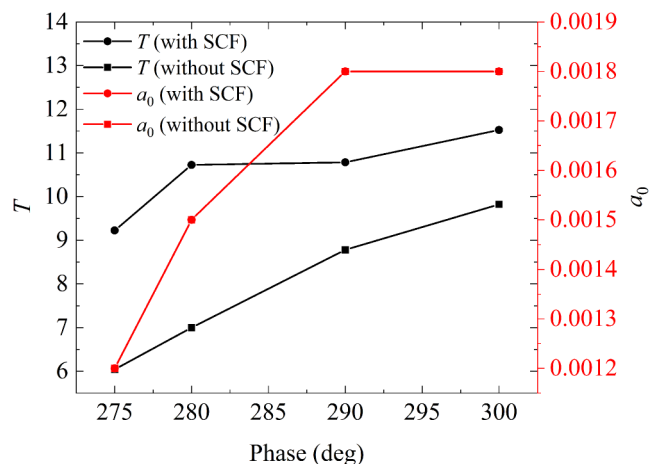


FIG. 7. The ratio of bunch spacing to RPL wavelength as a function of rf field phase with optimized laser power ( $E_{01} = 40 \text{ MV/m}$ ).

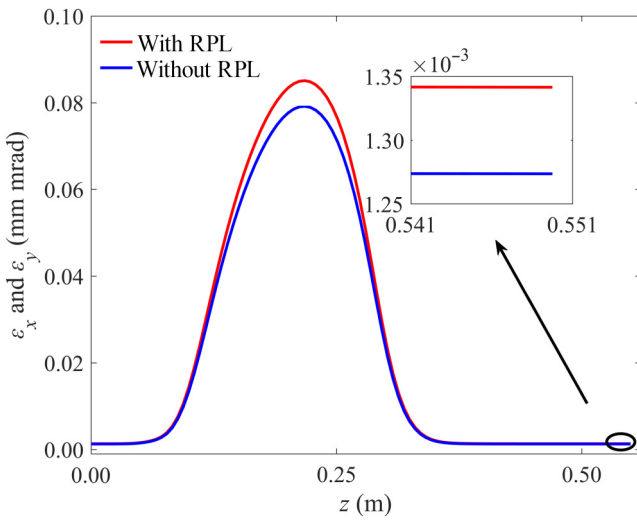


FIG. 8. Simulation results of the transverse emittance ( $E_{01} = 60 \text{ MV/m}$ ,  $\phi_{01} = 280^\circ$ ).

phase, respectively, with optimized laser power. The pulse length of the driving laser is 400 fs and the total bunch charge is set as 0.2 fC. The bunch spacing will change due to the space charge effect. Although the average energy of the electron beam varies from 2.84 to 1.18 MeV due to the changes of amplitude and phase of the rf field, the emittance of the electron beam can be basically the same. In these two figures, the optimized laser power is the same for the two cases with and without space charge force (SCF).

## V. APPLICABILITY AND KEY ASPECTS

To illustrate the applicability of this scheme, the influence of main parameters on the beam quality is

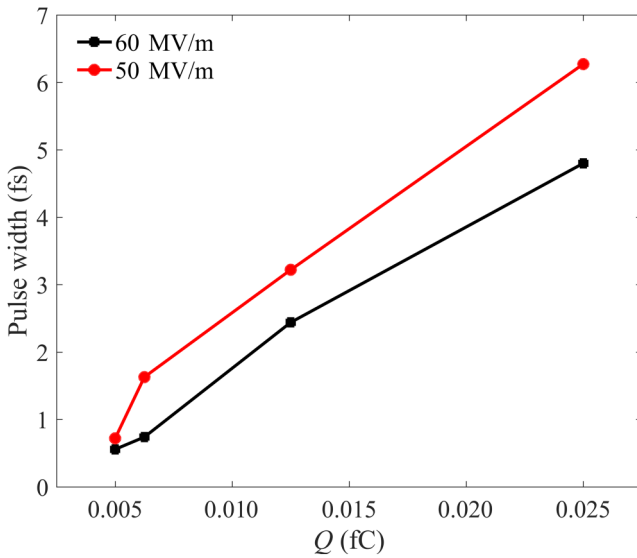


FIG. 9. Simulation results of the pulse width (FWHM) as a function of the bunch charge ( $\phi_{01} = 280^\circ$ ).

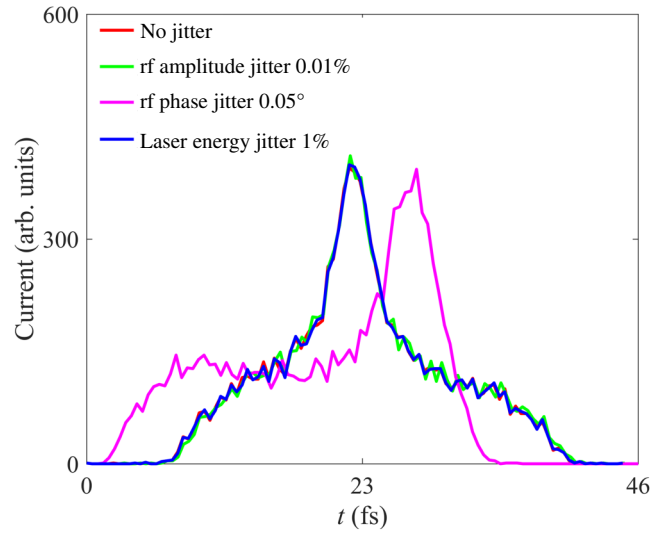


FIG. 10. Simulation result of the current distribution as influenced by the laser energy jitter, phase jitter, and rf amplitude jitter.

studied. The transverse emittance or brightness of the electron beam is the basic beam parameter that may indicate its utility for most applications. As seen in Fig. 8, the increase of normalized emittance caused by the RPL is only 5%. Using the normalized beam brightness calculation formula [26] given by  $B_n = [(2I)/(\pi^2 \varepsilon_x \varepsilon_y)]$ , where  $I$  is the peak current,  $\varepsilon_x$  is the normalized  $xx'$  trace space emittance, and  $\varepsilon_y$  is the normalized  $yy'$  trace space emittance, we get that the brightness is about 282 A/mm<sup>2</sup>mrad<sup>2</sup> for the electron beam shown in Fig. 5(b). The length of microbunches is another factor that affects application. As

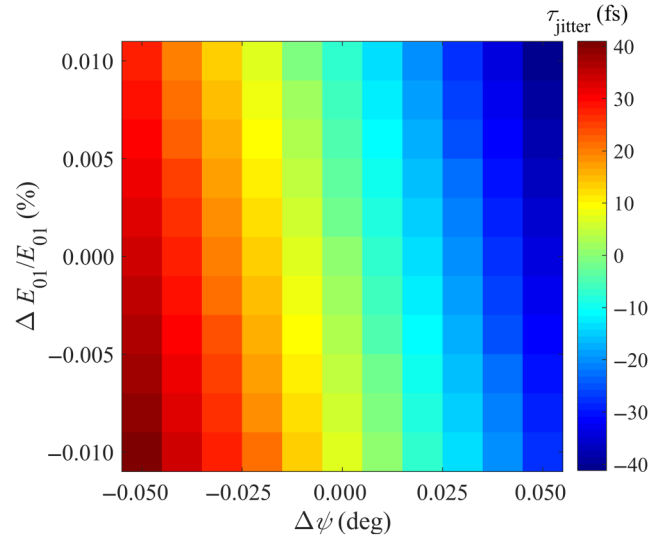


FIG. 11. Simulation result of the arrival time jitter at 0.55 m as influenced by the phase and rf amplitude fluctuation ( $E_{01} = 60 \text{ MV/m}$ ,  $\phi_{01} = 280^\circ$ ).

shown in Fig. 9, the pulse width is closely related to the bunch charge. To obtain a subfemtosecond electron bunch (rms), the amount of charge in a single microbunch should be lower than 0.01 fC.

Furthermore, the jitter of laser energy, rf phase, and rf field amplitude may also have an impact on the bunching result. As seen in Fig. 10, the critical factor is the phase jitter, which does not cause a change of pulse width, but makes the peak position being offset from the center of the bunch. For the application of MeV UED, the arrival time jitter, which is the fluctuation of the time of flight of the electron beam from the cathode to the sample, is a critical performance indicator. Obviously, the phase and amplitude jitter of the rf field will cause an energy fluctuation of the electron beam, which leads to an arrival time jitter. Figure 11 shows the simulation results of the arrival time jitter at 0.55 m (sample position) as influenced by the phase and rf amplitude fluctuation. The synchronization between laser and rf signal can be controlled to sub-10 fs rms [30], which corresponds to 0.01° phase jitter for a rf of 2856 MHz. With the help of low-level rf system, the long-term stability of the rf phase and amplitude can be further improved, and a beam energy fluctuation of  $6.57 \times 10^{-5}$  rms is achieved in SwissFEL [31]. By adopting the above technologies, the arrival time jitter of the proposed scheme can be about 5 fs, which might be further suppressed to a subfemtosecond level by using a bimodal rf gun [32] and a double-bend achromatic structure [18,19].

## VI. CONCLUSION

In summary, we have identified a regime to generate a relativistic attosecond electron pulse train and an isolated attosecond pulse in a photocathode rf gun. According to our study results, electron pulses of hundreds attoseconds in length can be generated by using a mature photocathode rf gun and commercial GW-power-level laser system. The emittance of the electron beam can be close to the initial thermal emittance, and the brightness can reach a level of  $100 \text{ A/mm}^2\text{mrad}^2$ . The proposed regime may enable existing MeV UED facilities to achieve a higher time resolution and open up many opportunities for other frontier researches that need ultrashort pulses, such as external injection in plasma acceleration, inverse Compton scattering x-ray sources, etc. In addition, for the attosecond pulse train, the tunability of the bunching wavelength will bring a solution for a more compact and tunable FEL source. We expect this regime to have a strong impact on future development of ultrashort-pulse electron-beam-based scientific facilities and applications.

## ACKNOWLEDGMENTS

This work is supported by the National Natural Science Foundation of China (11775216) and Youth Innovation Promotion Association (CAS).

- [1] J. Yang *et al.*, Imaging CF3I conical intersection and photodissociation dynamics with ultrafast electron diffraction, *Science* **361**, 64 (2018).
- [2] M. Z. Mo, Z. Chen, R. K. Li, M. Dunning, B. B. L. Witte, J. K. Baldwin, L. B. Fletcher, J. B. Kim, A. Ng, R. Redmer, A. H. Reid, P. Shekhar, X. Z. Shen, M. Shen, K. Sokolowski-Tinten, Y. Y. Tsui, Y. Q. Wang, Q. Zheng, X. J. Wang, and S. H. Glenzer, Heterogeneous to homogeneous melting transition visualized with ultrafast electron diffraction, *Science* **360**, 1451 (2018).
- [3] E. J. Sie *et al.*, An ultrafast symmetry switch in a weyl semimetal, *Nature* **565**, 61 (2019).
- [4] J. Yang, X. Zhu, J. P. F. Nunes, J. K. Yu, R. M. Parrish, T. J. A. Wolf, M. Centurion, M. Gühr, R. Li, Y. Liu, B. Moore, M. Niebuhr, S. Park, X. Shen, S. Weathersby, T. Weinacht, T. J. Martinez, and X. Wang, Simultaneous observation of nuclear and electronic dynamics by ultrafast electron diffraction, *Science* **368**, 885 (2020).
- [5] C. Pellegrini, A. Marinelli, and S. Reiche, The physics of x-ray free-electron lasers, *Rev. Mod. Phys.* **88**, 015006 (2016).
- [6] J. Yan *et al.*, Self-Amplification of Coherent Energy Modulation in Seeded Free-Electron Lasers, *Phys. Rev. Lett.* **126**, 084801 (2021).
- [7] S. Huang, Y. Ding, Z. Huang, and G. Marcus, Generation of subterawatt-attosecond pulses in a soft x-ray free-electron laser, *Phys. Rev. Accel. Beams* **19**, 080702 (2016).
- [8] P. M. Paul, E. S. Toma, P. Breger, G. Mullot, F. Augé, P. Balcou, H. G. Müller, and P. Agostini, Observation of a train of attosecond pulses from high harmonic generation, *Science* **292**, 1689 (2001).
- [9] G. Sansone, E. Benedetti, F. Calegari, C. Vozzi, L. Avaldi, R. Flammini, L. Poletto, P. Villoresi, C. Altucci, R. Velotta, S. Stagira, S. De Silvestri, and M. Nisoli, Isolated single-cycle attosecond pulses, *Science* **314**, 443 (2006).
- [10] K. E. Priebe, C. Rathje, S. V. Yalunin, T. Hohage, A. Feist, S. Schäfer, and C. Ropers, Attosecond electron pulse trains and quantum state reconstruction in ultrafast transmission electron microscopy, *Nat. Photonics* **11**, 793 (2017).
- [11] Y. Morimoto and P. Baum, Diffraction and microscopy with attosecond electron pulse trains, *Nat. Phys.* **14**, 252 (2018).
- [12] M. Kozák, N. Schönenberger, and P. Hommelhoff, Ponderomotive Generation and Detection of Attosecond Free-Electron Pulse Trains, *Phys. Rev. Lett.* **120**, 103203 (2018).
- [13] Y. Morimoto and P. Baum, Single-Cycle Optical Control of Beam Electrons, *Phys. Rev. Lett.* **125**, 193202 (2020).
- [14] M. Kozák, All-Optical Scheme for Generation of Isolated Attosecond Electron Pulses, *Phys. Rev. Lett.* **123**, 203202 (2019).
- [15] Y. X. Zhang, S. Rykovanov, M. Shi, C. L. Zhong, X. T. He, B. Qiao, and M. Zepf, Giant Isolated Attosecond Pulses from Two-Color Laser-Plasma Interactions, *Phys. Rev. Lett.* **124**, 114802 (2020).
- [16] C. Zhou, Y. Bai, L. Song, Y. Zeng, Y. Xu, D. Zhang, X. Lu, Y. Leng, J. Liu, Y. Tian, R. Li, and Z. Xu, Direct mapping of attosecond electron dynamics, *Nat. Photonics* **15**, 216 (2021).
- [17] C. Kealhofer, W. Schneider, D. Ehberger, A. Ryabov, F. Krausz, and P. Baum, All-optical control and metrology of electron pulses, *Science* **352**, 429 (2016).

- [18] F. Qi, Z. Ma, L. Zhao, Y. Cheng, W. Jiang, C. Lu, T. Jiang, D. Qian, Z. Wang, W. Zhang, P. Zhu, X. Zou, W. Wan, D. Xiang, and J. Zhang, Breaking 50 Femtosecond Resolution Barrier in MeV Ultrafast Electron Diffraction with a Double Bend Achromat Compressor, *Phys. Rev. Lett.* **124**, 134803 (2020).
- [19] H. W. Kim, N. A. Vinokurov, I. H. Baek, K. Y. Oang, M. H. Kim, Y. C. Kim, K.-H. Jang, K. Lee, S. H. Park, S. Park, J. Shin, J. Kim, F. Rotermund, S. Cho, T. Feurer, and Y. U. Jeong, Towards jitter-free ultrafast electron diffraction technology, *Nat. Photonics* **14**, 245 (2020).
- [20] C. Lu, T. Jiang, S. Liu, R. Wang, L. Zhao, P. Zhu, D. Xiang, and J. Zhang, Coulomb-Driven Relativistic Electron Beam Compression, *Phys. Rev. Lett.* **120**, 044801 (2018).
- [21] S. Carbajo, E. A. Nanni, L. J. Wong, G. Moriena, P. D. Keathley, G. Laurent, R. J. D. Miller, and F. X. Kärtner, Direct longitudinal laser acceleration of electrons in free space, *Phys. Rev. Accel. Beams* **19**, 021303 (2016).
- [22] S. Payeur, S. Fourmaux, B. E. Schmidt, J. P. MacLean, C. Tchervenkov, F. Legare, M. Piche, and J. C. Kieffer, Generation of a beam of fast electrons by tightly focusing a radially polarized ultrashort laser pulse, *Appl. Phys. Lett.* **101**, 041105 (2012).
- [23] N. Zaim, M. Thevenet, A. Lifschitz, and J. Faure, Relativistic Acceleration of Electrons Injected by a Plasma Mirror Into a Radially Polarized Laser Beam, *Phys. Rev. Lett.* **119**, 094801 (2017).
- [24] E. Esarey, P. Sprangle, and J. Krall, Laser acceleration of electrons in vacuum, *Phys. Rev. E* **52**, 5443 (1995).
- [25] Y. I. Salamin, Electron acceleration from rest in vacuum by an axicon Gaussian laser beam, *Phys. Rev. A* **73**, 043402 (2006).
- [26] T. Rao and D. H. Dowell, An engineering guide to photoinjectors, [arXiv:1403.7539](https://arxiv.org/abs/1403.7539).
- [27] S. Kajita, R. Yasuhara, M. Sato, N. Ohno, M. Tokitani, and N. Yoshida, Enhancement of multi-pulse laser induced damage threshold on Cu mirror under vacuum condition, *Opt. Express* **21**, 17275 (2013).
- [28] M. De Loos and S. Van Der Geer, in *5th European Particle Accelerator Conference* (JACow, Barcelona, Spain, 1996), p. 1241.
- [29] Y. Ding, A. Brachmann, F.-J. Decker, D. Dowell, P. Emma, J. Frisch, S. Gilevich, G. Hays, P. Hering, and Z. Huang *et al.*, Measurements and Simulations of Ultralow Emittance and Ultrashort Electron Beams in the Linac Coherent Light Source, *Phys. Rev. Lett.* **102**, 254801 (2009).
- [30] J. Kim, J. A. Cox, J. Chen, and F. X. Kärtner, Drift-free femtosecond timing synchronization of remote optical and microwave sources, *Nat. Photonics* **2**, 733 (2008).
- [31] Z.-Q. Geng, Beam-based optimization of swissFEL low-level RF system, *Nucl. Sci. Tech.* **29**, 1 (2018).
- [32] L. Wang, Y. Jiang, W. Fang, Z. Zhao, S. V. Shchelkunov, and J. L. Hirshfield, Simulation study of first and second harmonic photocathode bimodal gun, *Phys. Rev. Accel. Beams* **24**, 020401 (2021).